

## USING GRAVITATIONAL-WAVE STANDARD SIRENS

DANIEL E. HOLZ

Theoretical Division, Los Alamos National Laboratory, Los Alamos, NM 87545 and  
Kavli Institute for Cosmological Physics and Department of Astronomy & Astrophysics,  
The University of Chicago, Chicago, IL 60637

AND

SCOTT A. HUGHES

Department of Physics and Center for Space Research, Massachusetts Institute of Technology, 77 Massachusetts Avenue, Cambridge,  
MA 02139

*Draft version February 2, 2008*

### ABSTRACT

Gravitational waves (GWs) from supermassive binary black hole (BBH) inspirals are potentially powerful standard sirens (the GW analog to standard candles) (Schutz 1986, 2002). Because these systems are well-modeled, the space-based GW observatory *LISA* will be able to measure the luminosity distance (but not the redshift) to some distant massive BBH systems with 1–10% accuracy. This accuracy is largely limited by pointing error: GW sources generally are poorly localized on the sky. Localizing the binary independently (e.g., through association with an electromagnetic counterpart) greatly reduces this positional error. An electromagnetic counterpart may also allow determination of the event’s redshift. In this case, BBH coalescence would constitute an extremely precise (better than 1%) standard candle visible to high redshift. In practice, gravitational lensing degrades this precision, though the candle remains precise enough to provide useful information about the distance-redshift relation. Even if very rare, these GW standard sirens would complement, and increase confidence in, other standard candles.

*Subject headings:* black hole physics—gravitation—gravitational waves—galaxies: nuclei—cosmology: observations—cosmology: theory—gravitational lensing

### 1. INTRODUCTION

One of the major challenges to cosmology for the foreseeable future is to understand “dark energy”, the mysterious component responsible for the apparent accelerating expansion of our Universe (Riess et al. 1998; Perlmutter et al. 1999; Tonry et al. 2003; Knop et al. 2003). Dark energy can be parameterized by its contribution to the universe’s energy density,  $\Omega_X$ , and its equation-of-state ratio,  $w(z)$ . Of particular interest will be measurements that probe  $w(z)$ , testing whether the dark energy is a true cosmological constant [ $w(z) = -1$ ] or whether it arises, for example, from an evolving field (e.g. Caldwell, Dave, & Steinhardt 1998; Armendariz-Picon, Mukhanov, & Steinhardt 2000).

One of our best observational probes of the dark energy is the distance-redshift relation, which maps the expansion history of the universe. Much of our knowledge of this relation comes from observations of distant Type Ia supernovae (SNe). These SNe serve as standard candles: their observed intensity can be calibrated to tell us their luminosity distance,  $D_L$  (Phillips 1993; Riess, Press, & Kirshner 1995; Wang et al. 2003). As the redshift of a SN (or its host) can also be measured, each SN puts a point on the distance-redshift curve. Future surveys (e.g., *SuperNova/Acceleration Probe*<sup>1</sup>, *Large-aperture Synoptic Survey Telescope*<sup>2</sup>) are expected to measure thousands of Type Ia SNe, mapping the distance-redshift curve over a large span of redshift with good statistical significance.

Type Ia SNe are excellent standard candles, with a (calibrated) peak brightness thought to be known to about 15%. A possible objection to SNe as standard candles is the absence of a solid theoretical underpinning. Of particular concern is the possibility of evolution in SN brightnesses, leading to unknown systematic errors (Drell, Lored, & Wasserman 2000). In this article, we discuss a completely independent standard candle: the gravitational-wave (GW) driven inspiral of massive binary black holes (BBHs). As GW detections can be thought of as aural rather than optical (Hughes 2003), a more appropriate term for a GW standard candle is a “standard siren”.<sup>3</sup> Because BBH systems are relatively simple and well modeled (at least in the early “inspiral” phase of their coalescence), the GWs they generate determine the source’s luminosity distance with high accuracy: typically  $\delta D_L/D_L \sim 1\text{--}10\%$ , with most of the uncertainty arising from correlations with pointing errors (Hughes 2002). BBH merger events will follow the mergers of galaxies and pregalactic structures at high redshift (Volonteri, Haardt, & Madau 2003). Though the merger rate is poorly understood, *LISA* is expected to measure at least several events over its mission, especially as it is sensitive to these waves to enormous distances (Richstone 1998; Haehnelt 1998).

Since GWs do not provide the redshift of the source, BBH GW measurements alone do not probe the distance-redshift relation. However, as first noted by Bernard Schutz, should some kind of “electromagnetic” (EM) counterpart to a BBH GW event be identified, the situ-

<sup>1</sup> <http://snap.lbl.gov>

<sup>2</sup> <http://www.lsst.org>

<sup>3</sup> We thank Sterl Phinney and Sean Carroll for suggesting this term.

ation changes drastically (Schutz 1986, 2002). First, by determining the source position, many correlations which set the distance error are broken. The error then drops immensely — below 0.5–1% in many cases. Second, a counterpart could determine the source’s redshift. A BBH GW source coupled with an EM counterpart could therefore constitute an exceedingly good standard siren<sup>4</sup>. We comment at this point that, to date, there has not been a great deal of careful analysis regarding the nature of EM counterparts which may accompany a GW event. We discuss briefly some ideas that have been presented to date regarding the form that counterparts may take in §3 and §5. We hope that the promise of this high quality candle will motivate additional thinking on this issue.

In practice, gravitational lensing will limit the quality of this candle. GWs are lensed by intervening matter exactly as electromagnetic waves are lensed (Marković 1993; Wang, Stebbins, & Turner 1996; Takahashi & Nakamura 2003). As the waves propagate through our inhomogeneous universe, they are magnified (or demagnified), inducing some error in our inferred luminosity distance to the source. As we discuss in §4, the distribution of errors is such that a BBH candle will most likely be comparable in quality to a Type Ia SN standard candle. However — and we strongly emphasize this point — the BBH candle will have entirely different systematics from SNe. Concordance between the two types of measurement could thus alleviate concerns about evolutionary effects in Type Ia SNe, and greatly increase one’s confidence in all standard candles.

## 2. DISTANCE DETERMINATION WITH BBH GWS AND *LISA*

Massive BBH coalescences are among the most luminous events in the universe. That luminosity (peaked at  $\sim 10^{57}$  erg/sec) is radiated in GWs, which couple very weakly to matter. The planned space-based GW detector *LISA* (the *Laser Interferometer Space Antenna*) will be sensitive to these BBH waves in the frequency band ( $10^{-5}$ – $10^{-4}$ ) Hz  $\lesssim f \lesssim 0.1$  Hz, making possible measurements from binaries with total masses  $m_1 + m_2 \sim 10^3$ – $10^6 M_\odot$  (Danzmann 1998) out to redshifts of at least  $z \sim 5$ – $10$  and possibly beyond (Hughes 2002; Vecchio 2004). In this section we discuss how *LISA* measurements determine the distance to a source, summarizing our model of the waveform and *LISA*’s sensitivity and response, and discussing the measurement precision we expect from measuring merging black hole populations.

### 2.1. Merging black hole GWs

For this paper, the most interesting epoch of BBH coalescence is the *inspiral*, when the binary’s members are widely separated and slowly spiral together due to back-reaction from GW emission. The GWs from this epoch are well modeled using the post-Newtonian approximation

<sup>4</sup> It may also be possible to use the *distributions* of observed binaries for cosmology, obviating the need for an EM counterpart (Chernoff & Finn 1993; Finn 1996; Wang & Turner 1997). Unless the event rate is much higher than currently expected, however, the statistical errors associated with these distributions suggest that these methods will not achieve accuracy sufficient to measure properties of the dark energy equation of state, our primary focus. Certainly other cosmologically interesting measurements could be made.

of a binary’s members; see Blanchet (2002) and references therein for more detailed discussion. We will not discuss waves from the *merger* (in which the holes come into contact, forming a single body), nor from the *ring-down* (the final, simple stage of the ringdown, in which the merged binary is well-modeled as a single, distorted black hole), as they do not substantially impact distance determination.

Inspiral GWs encode the luminosity distance to a binary, its position on the sky, its orientation, and information about certain combinations of masses and spins; see Arun *et al.* (2004) and Blanchet *et al.* (2004) for up-to-date discussion and details. The inspiral does *not* encode a source’s cosmological redshift. Redshift is instead entangled with the binary’s evolution. For example, the masses ( $m_1, m_2$ ) impact orbital evolution as timescales ( $Gm_1/c^3, Gm_2/c^3$ ). These timescales redshift, so the measured masses redshift: a binary with masses ( $m_1, m_2$ ) at redshift  $z$  is indistinguishable from a local binary with masses  $[(1+z)m_1, (1+z)m_2]$  (modulo amplitude). This reflects the fact that general relativity has no absolute scale.

In a reference frame centered on the solar system’s barycenter, the strongest harmonic of the inspiral GW’s two polarizations has the form

$$h_+ = \frac{2\mathcal{M}_z^{5/3}[\pi f(t)]^{2/3}}{D_L} \left[ 1 + (\hat{L} \cdot \hat{n})^2 \right] \cos[\Phi(t)], \quad (1)$$

$$h_\times = \frac{4\mathcal{M}_z^{5/3}[\pi f(t)]^{2/3}(\hat{L} \cdot \hat{n})}{D_L} \sin[\Phi(t)]. \quad (2)$$

The mass parameter  $\mathcal{M}_z = (1+z)(m_1 m_2)^{3/5}/(m_1 + m_2)^{1/5}$  is the binary’s redshifted “chirp mass”, so called because it largely sets the rate at which the binary’s members spiral towards one another, determining the “chirp” of the orbital frequency. The phase  $\Phi(t)$  depends on intrinsic binary parameters — the masses and spins of its members (e.g., Poisson & Will 1995). It depends particularly strongly on  $\mathcal{M}_z$ ; as a consequence, phase coherent measurements of the waves will determine the chirp mass with great precision (Finn & Chernoff 1993; Cutler & Flanagan 1994). The wave frequency  $f(t) = (1/2\pi)d\Phi/dt$ . The unit vector  $\hat{n}$  points from the center of the barycenter frame to the system, and hence defines its position on the sky;  $\hat{L}$  points along the binary’s orbital angular momentum, and hence defines its orientation. Notice that the luminosity distance  $D_L$  appears in combination with these two angular factors. Determining  $D_L$  thus requires fixing these angles. As we now discuss, *LISA* is able to do so by virtue of its orbital motion.

### 2.2. Merger GWs as measured by *LISA*

The *LISA* antenna consists of three spacecraft, arranged in orbits about the Sun such that they form an equilateral triangle (roughly; the armlengths are in general not equal, and in fact oscillate — albeit with periods much longer than that of the GWs we aim to observe). This triangle “rolls” as the spacecraft move through their individual orbits, preserving the triangular formation. The centroid of the constellation shares Earth’s orbit, lagging by  $20^\circ$ , so that it takes 1 year to orbit the Sun. Figure 1 shows a schematic of the orbital configuration.

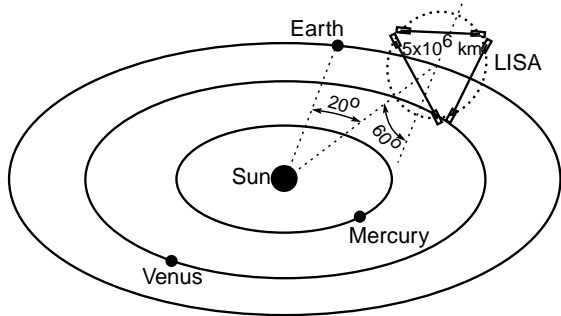


FIG. 1.— Illustration of the *LISA* antenna’s orbit. The constellation “rolls” as its centroid orbits the sun, completing one full revolution for each orbit.

See Danzmann (1998) for detailed discussion of the *LISA* mission and its orbital configuration.

At least in the low frequency limit ( $f < c/L$ , where  $L$  is armlength), *LISA* can very usefully be regarded as two GW detectors: the time varying armlength data,  $(\delta L_1, \delta L_2, \delta L_3)$  can be used to synthesize outputs for two equivalent “L”-shaped detectors, with  $90^\circ$  arms. These “equivalent detectors” are rotated by  $45^\circ$  with respect to one another; see Cutler (1998) for details and derivation of this viewpoint. The datastream  $s_{I,II}$  of these two equivalent detectors is given by a weighted sum of the two GW polarizations, plus noise:

$$s_{I,II}(t) = \frac{\sqrt{3}}{2} \left[ F_{I,II}^+(t) h_+(t) + F_{I,II}^\times(t) h_\times(t) \right] + n_{I,II}(t). \quad (3)$$

The prefactor  $\sqrt{3}/2$  in this expression enters when converting the “real” interferometer response to that of the synthesized equivalent detectors. The antenna functions  $F_{I,II}^{+,\times}$  depend on the orientation and position of the source relative to the antenna. Because of the antenna’s orbital motion, the position and orientation of the source relative to the antenna is continually changing. The motion of the detector thus modulates the measured signal; the exact nature of the modulation depends upon the position and orientation of the source. We write the response functions as time dependent functions to reflect this modulation. Note also that the waveform phasing is modified in an important manner by the antenna’s motion — the orbital motion causes frequency as well as amplitude modulation. See Cutler (1998) for further discussion.

We take the noises in the equivalent detectors,  $n_{I,II}(t)$ , to be uncorrelated, Gaussian random processes, with the same RMS values:

$$\langle n_{I,II} \rangle = 0; \quad \langle n_I^2 \rangle = \langle n_{II}^2 \rangle. \quad (4)$$

In all of our analysis, we use the same noise model as that used by Barack & Cutler (2004) [their Eqs. (48)–(54)]. In our calculations, it is necessary to introduce a low frequency cutoff — a frequency at which the sensitivity to GWs rapidly degrades. This cutoff has important implications for determining which binaries *LISA* can measure: the frequency support of a binary’s GW spectrum is inversely proportional to its mass. In other words, more massive binaries will radiate at lower frequencies than less massive binaries. The low frequency cutoff thus determines the *maximum* binary black hole

mass accessible to *LISA* measurements. It also determines the amount of time for which a binary’s waves are in band: a binary that may only be in band for a few days when  $f_{\text{low}} = 10^{-4}$  Hz may be in band for many months when  $f_{\text{low}} = 3 \times 10^{-5}$  Hz.

Unless stated otherwise, we have set  $f_{\text{low}} = 10^{-4}$  Hz for the results we present here. This is a somewhat conservative choice; some members of the *LISA* mission design community (particularly P. Bender) argue that *LISA* should have good sensitivity down to frequencies  $f \sim 10^{-5}$  Hz. Accordingly, we have put  $f_{\text{low}} = 3 \times 10^{-5}$  Hz in several of our calculations. We flag such cases when appropriate.

To understand more clearly how *LISA* extracts the luminosity distance from measurements of a binary black hole inspiral, it is useful to rewrite somewhat schematically the measured form of the inspiral as follows:

$$h_{I,II}^{\text{meas}}(t) = \frac{\mathcal{M}_z^{5/3} f(t)^{2/3}}{D_L} \mathcal{F}_{I,II}(\text{“angles”}, t) \cos[\Phi(t) + \varphi_{I,II}(\text{“angles”}, t)] \quad (5)$$

We have subsumed the angle-dependent factors  $(\hat{L} \cdot \hat{n})$  and  $F_{I,II}^{+,\times}$  into the schematic functions  $\mathcal{F}_{I,II}(\text{“angles”}, t)$ ; we leave the dependence upon  $t$  in these functions as a reminder that the constellation’s motion modulates the waveform. We have likewise written the phase modulations imposed by the detector’s response and motion in the schematic form  $\varphi_{I,II}(\text{“angles”}, t)$ .

From the form of equation (5) we see that the luminosity distance is very strongly correlated with the redshifted chirp mass,  $\mathcal{M}_z$ , and the various angles which set the instantaneous waveform amplitude. As already mentioned,  $\mathcal{M}_z$  is typically determined with extremely high precision because it fixes the phase evolution: typically,  $\delta \mathcal{M}_z / \mathcal{M}_z \lesssim 0.01\%$ . See Hughes (2002), Vecchio (2004) for examples specific to *LISA*.

The modulations induced by *LISA*’s orbital motion make it possible to measure sky position for events which last for at least a fair fraction of *LISA*’s orbit. We estimate the accuracy with which position (among other parameters) is determined using a maximum likelihood parameter estimation formalism (Finn 1992): from the detector’s response to a given gravitational wave, we construct the variance-covariance matrix  $\Sigma^{ab}$ . Diagonal elements of this matrix represent the rms error  $\langle (\delta \chi^a)^2 \rangle$  in a source parameter  $\chi^a$ ; off-diagonal components describe the degree to which errors in parameters  $\chi^a$  and  $\chi^b$  are correlated. See Hughes (2002) for discussion specifically tailored to this application.

### 2.3. Measurement accuracy distributions

To assess distance and position accuracy, we have estimated the accuracy with which these parameters are measured for a wide range of binary masses. For each set of masses, we randomly distribute the sky position and orientation of 10,000 such binaries. We then calculate the fractional accuracy with which distance is determined for each binary,  $\delta D_L / D_L$ , as well as the angular sky position error  $\delta \theta$ . Figure 2 shows the distribution we find in these quantities for binaries with  $m_1 = 10^5 M_\odot$ ,  $m_2 = 6 \times 10^5 M_\odot$  at  $z = 1$ . We find that the typical position determination is relatively poor — these binaries are fixed to an error box that, at best, is  $\sim 5$  arcminutes

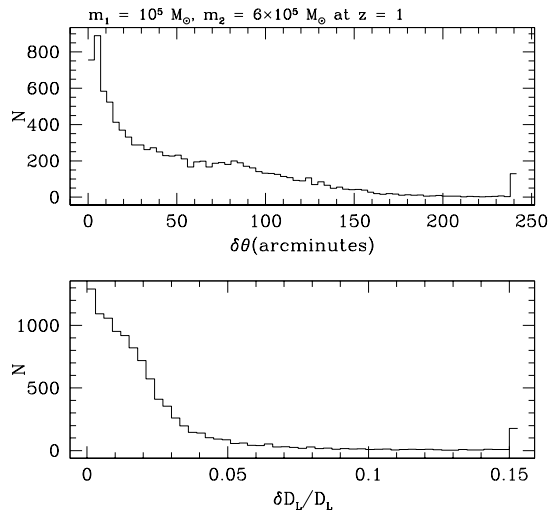


FIG. 2.— Pointing and distance error distributions for measurements at  $z = 1$  of a binary of masses  $m_1 = 10^5 M_\odot$ ,  $m_2 = 6 \times 10^5 M_\odot$ . These distributions were made by Monte-Carlo simulations of 10,000 *LISA* BBH measurements, randomly distributing the binaries’ positions, orientations, and merger times; see Hughes (2002) for details. The top distribution shows that the most likely position error boxes have sides  $\delta\theta \lesssim 10$  arcminutes, spreading out to  $\delta\theta \gtrsim 3^\circ$ . The distance distribution peaks at  $\delta D_L/D_L \lesssim 1\%$ , with most of the distribution confined to  $\delta D_L/D_L \lesssim 5\%$ .

on a side. In most cases, the resolution is substantially worse. The distance determination, by contrast, is quite good: half of these events have their distance determined with precision  $\delta D_L/D_L \lesssim 1\%$ .

Table 1 summarizes the parameter determination distributions we find for a wide range of masses. For  $\delta D_L/D_L$  and  $\delta\theta$ , we give the 5%, 25%, 50%, and 90% likelihood values from the distributions predicted by our Monte-Carlo calculation. For example, for binaries with  $m_1 = 3 \times 10^4 M_\odot$ ,  $m_2 = 10^5 M_\odot$  at  $z = 1$ , 25% of all events have  $\delta D_L/D_L \lesssim 0.006$  and localize the source to  $\delta\theta \lesssim 14.6$  arcminutes; 90% of all events with these masses and redshifts have  $\delta D_L/D_L \lesssim 0.029$  and localize the source to  $\delta\theta \lesssim 120$  arcminutes.

Notice that, in this table, the best pointing and distance determination occurs for binaries that have a total (redshifted) mass  $(1+z)(m_1+m_2) \simeq \text{several} \times 10^5 M_\odot$ . Two competing effects drive this behavior. First, for small binaries the amplitude of the GWs is smaller; the degradation of their parameter determination is due to reduced signal-to-noise ratio. Larger binaries are more interesting. When such binaries enter *LISA*’s sensitive band, they are closer to their final merger — much less inspiral remains once *LISA* begins measuring their waves. They therefore do not exhibit as many cycles of detector-motion-induced modulation, and so their position angles are not as well determined. In particular, we find that distance and position determination rapidly degrades as binaries are made more massive than  $(1+z)(m_1+m_2) \gtrsim \text{a few} \times 10^6 M_\odot$ .

The poor parameter determination tendency of large binaries can be repaired somewhat by improving *LISA*’s low frequency sensitivity. If the antenna has good sensitivity at lower frequencies, the span of data containing

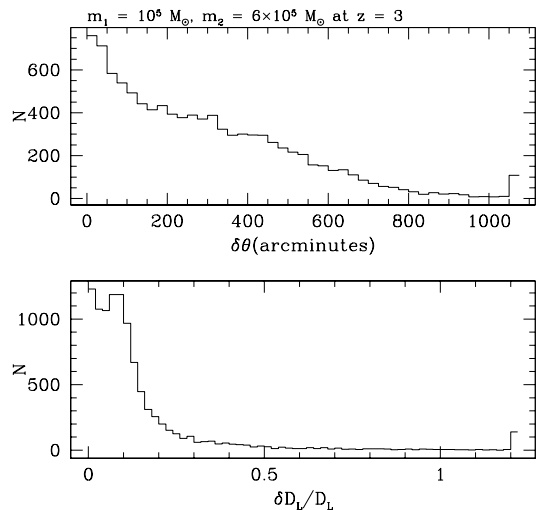


FIG. 3.— Pointing and distance error distributions for measurements at  $z = 3$  of a binary of masses  $m_1 = 10^5 M_\odot$ ,  $m_2 = 6 \times 10^5 M_\odot$ . The distribution for position error is so broad that we cannot really identify a “most likely” position error; however, most of the distribution lies at  $\delta\theta \lesssim 10^\circ$ . The distance distribution peaks at  $\delta D_L/D_L \lesssim 10\%$ , with most of the distribution confined to  $\delta D_L/D_L \lesssim 30\%$ .

good information about the inspiral can be lengthened. Table 2 shows how well we measure distance and position when  $f_{\text{low}}$  is reduced from  $10^{-4}$  Hz to  $3 \times 10^{-5}$  Hz. We now find that the distance is determined very precisely for binaries with total mass (several)  $\times 10^6 M_\odot$ . Sky position error is no worse than that achieved at lower masses —  $\delta\theta \lesssim 10$  arcminutes in the best cases, and is more typically a factor of a few larger than this.

The same general story holds as we move to larger redshift. Figure 3 duplicates the content of Figure 2, but with binaries at redshift  $z = 3$ . Likewise, Tables 3 and 4 duplicate the content of Tables 1 and 2, respectively, with all binaries placed at  $z = 3$ . The overall parameter determinations are worsened, as we would expect — these sources are much farther away, and so have greatly reduced signal-to-noise. In addition, the larger cosmological redshift shifts the signal to lower frequencies, where much of it is lost in low-frequency noise. To quantify the impact of this effect, in Table 4 we present results showing what happens when we lower  $f_{\text{low}}$  from  $10^{-4}$  Hz to  $3 \times 10^{-5}$  Hz. All cases with  $m_1+m_2 \gtrsim 6 \times 10^5 M_\odot$  are substantially improved by this fix. Good low frequency performance will be important for measuring high redshift binaries. The best pointing accuracy we find is  $\delta\theta \lesssim 40$  arcminutes;  $\delta\theta \sim 1^\circ$  or larger is more typical. The luminosity distance can still be determined quite well — we find errors of a few percent in the best cases, and  $\delta D_L/D_L \lesssim 15\%$  is quite common.

It is worth emphasizing at this point that the results we present here are most likely somewhat conservative. By taking into account other GW harmonics (Moore & Hellings 2002) and properly accounting for the high-frequency structure of *LISA*’s response (Seto 2002), the pointing accuracy, and thus distance accuracy, can be improved by a factor of a few. Properly accounting for modulations induced by spin-orbit and spin-spin cou-

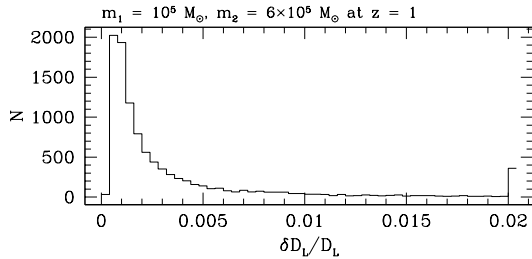


FIG. 4.— Distance errors for BBH measurements at  $z = 1$  with  $m_1 = 10^5 M_\odot$ ,  $m_2 = 6 \times 10^5 M_\odot$ , assuming that an electromagnetic counterpart allows precise sky position determination. The peak error is at  $\delta D_L/D_L \sim 0.1\%$ , and is almost entirely confined to  $\delta D_L/D_L \lesssim 0.5\%$ .

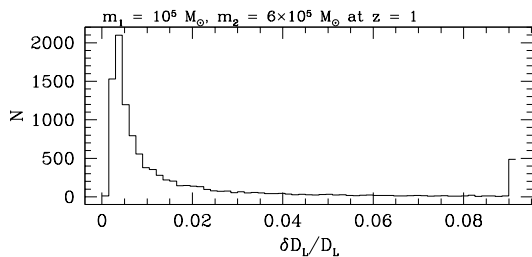


FIG. 5.— Distance errors for BBH measurements at  $z = 3$  with  $m_1 = 10^5 M_\odot$ ,  $m_2 = 6 \times 10^5 M_\odot$ , assuming that an electromagnetic counterpart allows precise sky position determination. The peak error is at  $\delta D_L/D_L \sim 0.5\%$ , and is almost entirely confined to  $\delta D_L/D_L \lesssim 2\%$ .

pling can also improve pointing accuracy and thus distance determination, in some cases significantly (Vecchio 2004).

Using a determination of  $D_L$ , we can *infer* the redshift by using knowledge of the universe’s geometry (the Hubble constant, mean density of matter  $\Omega_m$ , and density of dark energy  $\Omega_X$ ) (Hughes 2002). This makes possible interesting analyses (e.g., we can map the distribution of black hole masses as a function of redshift), but presupposes rather than measures the distance-redshift relation.

### 3. THE IMPACT OF A COUNTERPART

Parameter estimation improves dramatically when an EM counterpart to a BBH GW event can be identified. The counterpart will almost certainly be pinpointed with far greater accuracy than is possible with GWs. Correlations between position and distance are then broken, greatly reducing the distance error. An example of this improvement is shown for  $z = 1$  in Figure 4. The distribution of distance errors peaks near  $\delta D_L/D_L \sim 0.1\%$ , and is largely confined to  $\delta D_L/D_L \lesssim 1\%$ . Similar results are seen for  $z = 3$  (Fig. 5), albeit with precision degraded by a factor of a few due to lower signal-to-noise. Comparing to the lower panel of Figures 2 and 3, we see that associating the event with a counterpart improves distance accuracy by roughly an order of magnitude. This rough level of improvement holds over a wide band of mass and redshift.

A correlated GW/EM measurement will be particularly important if the counterpart provides a redshift as

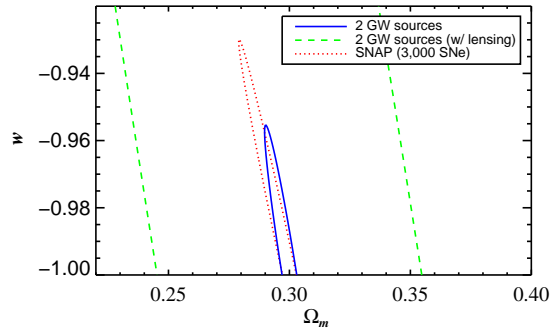


FIG. 6.— Likelihood contours for measurement of the matter density  $\Omega_m$  and dark energy equation of state parameter  $w$  (with the pressure and density of the dark energy related by  $p = w\rho$ ). We assume that the universe is flat, and that the underlying model has  $\Omega_m = 0.3$  and  $w = -1$ . The two GW sources are at  $z = 1$  and  $z = 3$ , while the SNAP SNe are evenly distributed within  $0.7 < z < 1.7$ .

well as an improved  $D_L$ . Such a measurement would constitute a powerful standard candle, probing the distance-redshift relation in a manner complementary to other candles, such as Type Ia supernovae. Assuming a flat universe and a Hubble constant  $h_0 = 0.65$ , we ask how well the matter density  $\Omega_m$  and dark energy equation-of-state ratio  $w$  can be measured. Figure 6 shows estimated likelihood contours ( $1-\sigma$ ) in the  $(\Omega_m, w)$  plane. The dotted line shows the contour expected for measurements of 3,000 SNe evenly distributed within  $0.7 < z < 1.7$  (reasonable choices for *SNAP*); the solid contour is for two GW events, one each at  $z = 1$  and  $z = 3$ . (We will discuss the dashed line further below.) Redshift and distance are measured with such accuracy that the contours are extremely tight even for only a small number of sources.

We emphasize the current poor understanding of EM counterparts to BBH GW events, although the possibility of such counterparts has been discussed for quite some time (e.g., Begelman, Blandford, & Rees 1980). Milosavljević & Phinney (2004) have recently examined the evolution of gas in the environment of a merging binary, and show that there is likely to be a delayed electromagnetic afterglow. They find that the merging binary carves a hollow region in the volume of circumbinary gas. The binary separation shrinks faster than the inner edge of the hollowed region; thus, as the coalescence proceeds, there should be no substantial accretion of material onto the system. The gas falls onto the merged remnant several years after the merger, leading to an afterglow that should be measurable by next generation x-ray telescopes.

Other models suggest that there may be an electromagnetic *precursor* to the merger, rather than a delayed glow. One example is discussed by Armitage & Natarajan (2002). They argue that gas is driven onto the larger member of the binary by the secondary’s inspiral, leading to super-Eddington accretion. In this model, much of the inner disk may be expelled from the system in a high velocity ( $\sim 10^4$  km/sec) outflow. Such strong outflows could flag a recent or impending merger. A similar family of models (Sillanpää et al. 1988; Lehto & Valtonen 1996) explains periodic variations in the BL Lac object OJ 287 by a tight, eccentric binary system with mass ratio of

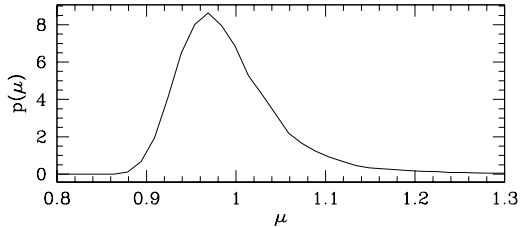


FIG. 7.— The differential probability of magnification by gravitational lensing,  $p(\mu)$ , for sources at  $z = 1.5$  in a concordance universe; see Wang, Holz, & Munshi (2002) for details.

about 1:100. Flaring outbursts from this quasar are explained as arising from the secondary periodic crossing of the primary’s accretion disk. Given the great payoff that would follow from associating a counterpart to a GW event, we strongly advocate continuing to develop and refine models of BBH mergers.

It is worth noting that, for a small fraction of binaries (assuming a sufficiently high event rate), *LISA* will provide an error box of  $\lesssim 5$  arcmin, and an estimate of the time of merger about a day in advance. Regardless of the state of theoretical predictions, we imagine that in such cases there will be great interest in searching the GW source error box for any observational counterparts to the merger. Indeed, as we briefly discuss in §5, the number of relevant galaxies in the *LISA* error box may be fairly small, and so associating an EM counterpart to the GW event may be tractable.

#### 4. GRAVITATIONAL LENSING

Having discussed the impressive quality of GW standard sirens, we turn now to an important caveat: the impact of gravitational lensing on the distance measurement. GWs are lensed exactly as EM radiation is lensed. Since we expect BBH events to come from rather large redshift ( $z \gtrsim 1$ ), weak lensing in the GW datasets should be common (Marković 1993; Wang, Stebbins, & Turner 1996) (in addition to the occasional strongly-lensed source).

A lens with magnification  $\mu$  will distort the inferred luminosity distance to the source: if the true distance is  $D_L$ , we measure  $D_L/\sqrt{\mu}$ , incurring a “systematic” error  $\Delta D_L/D_L = 1 - 1/\sqrt{\mu}$ . We estimate the error such lensing is likely to introduce by convolving this quantity with the expected magnification distribution,  $p(\mu)$  (Holz & Wald 1998; Wang, Holz, & Munshi 2002); an example of this distribution is shown in Figure 7. Using parameters appropriate to a  $\Lambda$ CDM model of the universe, we find a mean error at  $z = 2$  of  $\langle \Delta D_L/D_L \rangle \simeq 0.005$ , with a variance  $\sqrt{\langle (\Delta D_L/D_L)^2 \rangle} \simeq 0.09$  (approximating the lensing by a Gaussian; see Holz & Linder (2005)). The dashed line in Figure 6 shows the contour we expect from the 2 GW sources when lensing errors are included. The parameter accuracies are significantly degraded.

Of course, this magnification bias affects *all* standard candles, not just GWs. The rate of Type Ia SNe, however, is high enough to sufficiently sample the entire lensing distribution, and thus average away the bias. Missions such as *SNAP* are designed to observe thousands of SNe at high redshift, in large part to overcome gravi-

tational lensing. Indeed, this may allow one to measure the lensing signal well enough to infer characteristics of the lensing matter (Metcalf & Silk 1999; Seljak & Holz 1999). This is unlikely to be the case with BBH GWs: the rate of mergers will likely be much lower than that of SNe (Richstone 1998; Haehnelt 1998), so we cannot count on enormous numbers of events. We also emphasize that we do not expect to be able to correct for gravitational lensing effects on a case-by-case basis (Dalal et al. 2003). Lensing, therefore, will introduce an insurmountable error of  $\sim 5$ –10% for each individual high redshift event, significantly greater than the intrinsic distance error.

#### 5. IDENTIFYING THE COUNTERPART

In order to provide data on the distance-redshift curve, a GW event must be associated with an “electromagnetic” counterpart — GWs provide an accurate measure of luminosity distance, but give no direct information about redshift. This is the weakest link in our analysis: we do not know whether such counterparts exist. However, a simple counting argument suggests that the number of relevant galaxies in the *LISA* error cube may be fairly small. We approximate the redshift distribution of source galaxies by

$$\frac{dN}{dRd\Omega} \propto R^\alpha \exp[-(R/R_*)^\beta], \quad (6)$$

where  $R$  is the comoving distance; we take  $\alpha = 1$ ,  $\beta = 4$ , and  $R_* = c/H_0$  (Kaiser 1992; Hu 1999). We normalize this to a projected number density of

$$\frac{dN}{d\Omega} = \int dR \frac{dN}{dRd\Omega} \simeq 300 \text{ galaxies/arcmin}^2, \quad (7)$$

approximating the Hubble Deep Field (Williams, et al. 1996).

As we have discussed extensively, a GW measurement of a binary black hole merger determines the position on the sky to within some error  $\delta\theta$ , and determines the luminosity distance to within some error  $\delta D_L$ . By assuming a cosmological model we can convert the measured luminosity distance, and its error, to any other desired cosmic distance measure. Denoting by  $\delta R(\delta D_L; \delta \text{cosmology})$  the error in comoving distance due to both the GW measurement error and the uncertainty in cosmological parameters, the number of galaxies which lie in the 3-dimensional GW error cube is

$$N_{\text{error cube}} \simeq \frac{dN}{dRd\Omega} \times \delta\theta^2 \delta R(\delta D_L; \delta \text{cosmology}). \quad (8)$$

Figure 8 shows four realizations of  $N_{\text{error cube}}$  as a function of GW event redshift,  $z$ . We have scaled to a near best-case pointing accuracy of  $\delta\theta = 1$  arcmin; we emphasize that this is an optimistic, though not implausible, pointing error. From the Tables it is apparent that about 5% of binaries with masses and redshifts in the *LISA* sweetspot have positional errors  $\delta\theta \lesssim 5$  arcmin. As discussed towards the end of §2.3, these results may be conservative — accounting for spin-induced precessional effects may allow certain degeneracies to be broken and improve *LISA*’s pointing accuracy (Vecchio 2004). [A fiducial pointing error of 1 arcminute also makes it very simple, by Eq. (8), to scale to larger values.] The number of galaxies decreases significantly as uncertainties in cosmological parameters are reduced (as is to be expected by

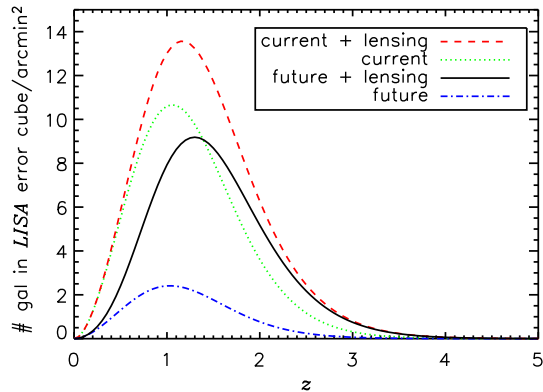


FIG. 8.— Number of candidate host galaxies per square arcmin of *LISA* error cube for a supermassive binary black hole coalescence event, as a function of redshift of the event. Dotted (green) line utilizes current uncertainties in cosmological parameters (Spergel et al. 2003). Dash-dotted (blue) line represents possible future improvements in these parameters (1% in  $\Omega_m$ ,  $\Omega_\Lambda$ ,  $h_0$ ). Dashed (red) line includes the degradation in the depth of the error cube due to gravitational lensing, for current cosmological uncertainties. Solid (black) line represents future cosmological uncertainties, with the inclusion of gravitational lensing degradation. The 1 arcmin *LISA* sky position error considered here is optimistic, though not implausible (see text). This choice allows for a straightforward scaling of the curves to larger positional errors.

the time that *LISA* is operating). In Figure 8 we include the curve for the current state of errors on cosmological parameters, as well as for expected future, percent-level, measurements. As was discussed in the previous section, gravitational lensing adds a further, insurmountable error to the GW measurement of  $\delta D_L$ . We approximate the lensing effects by a Gaussian in magnification, with variance given by  $\sigma_{\text{lensing}} = 0.088z$  (Holz & Linder 2005). Although this expression is strictly appropriate only for high source statistics (as otherwise the lensing distribution is non-Gaussian), it is a sufficiently good approximation for present purposes. With the inclusion of lensing errors in addition to cosmological parameter uncertainties, we find  $\lesssim 10$ – $20$  potential counterpart galaxies in 1 arcmin of *LISA* error cube.

The number of candidate host objects for a galactic binary black hole merger is thus likely to be tractable. What remains is to find a way to identify which of the dozen or so candidate objects is in fact the host of the merger. Useful models exploring the signatures that may constitute “precursors” of the merger exist (Armitage & Natarajan 2002; Sillanpää et al. 1988; Lehto & Valtonen 1996); we are hopeful that such models can be extended to the ranges of mass and mass ratio of binaries that are likely to be observationally interesting to *LISA*.

The remnant of the merger is very likely to have an irregular morphology. In addition, the host galaxy may be in an active phase. Milosavljević & Phinney (2004) have recently developed a model for the late x-ray afterglow of a BBH merger. Kocsis et al. (2005) consider a scenario in which a merger remnant is associated with a quasar, and argue that in this case the paucity of quasars will make the identification of a counterpart significantly easier. In both of these models the merger remnant “lights up”, and is thus relatively easy to identify in the positional error box. Even if the remnant does not light up,

other information will help winnow the list of candidate host galaxies. For example, the GWs will measure the masses of the black holes with good accuracy; by using properties such as the  $M_{\text{BH}}-\sigma$  relation we can estimate specific properties (e.g., kinematics, luminosity) that the host galaxy would be expected to have.

Observations of the *LISA* error boxes will no doubt be undertaken, regardless of the state of theoretical predictions. It is only by such direct observations that we will determine whether or not EM counterparts to BBH GW sources can be identified.

## 6. CONCLUSIONS

Because of their potential as an independent set of standard candles, BBH GW standard sirens can make an important contribution to programs to map the distance-redshift relation over a large span of redshift. Although the intrinsic precision of these candles is phenomenal, this precision will be limited in practice because of gravitational lensing. With lensing taken into account, the accuracy of the BBH GW candle is comparable to (or perhaps slightly better than) a Type Ia SN. It is sobering to note that we are already approaching the point at which lensing, rather than intrinsic dispersion, limits our ability to use standard candles.

We emphasize that the systematics of BBH events are entirely different from those of Type Ia SNe. As such, the greatest impact of BBH standard sirens may be to verify, and thereby increase our confidence in, other standard candles. The utility of these GW standard sirens depends on the identification of an electromagnetic counterpart, through which a redshift to the source can be determined. It is not unlikely that, at least for some of the best-observed systems, a counterpart will be found. If this is the case, the BBH GW source would become an exceptionally precise standard siren.

We thank Zoltan Haiman, Kristen Menou, Steinn Sigurdsson, and particularly Shane Larson for useful discussions; we also thank Sam Finn for detailed and helpful comments on a previous version of this manuscript. We thank Sean Carroll and Sterl Phinney for independently suggesting that the gravitational-wave analogue of the standard candle be named the “standard siren”. We are extremely grateful to Emanuele Berti for pointing out that the speed of the Monte-Carlo code used in this analysis could be vastly improved by changing our integration routines. Finally, we thank the referee for suggesting that morphological characteristics and the  $M_{\text{BH}}-\sigma$  relation may help to identify a merger event’s host galaxy. This work was initiated when the authors were at the Kavli Institute for Theoretical Physics (Santa Barbara), and were supported by NSF Grant PHY-9907949. DEH is supported by NSF Grant PHY-0114422, and gratefully acknowledges a Feynman Fellowship from LANL. SAH is supported by NASA Grant NAG5-12906 and NSF Grant PHY-0244424.

## REFERENCES

- Armendariz-Picon, C., Mukhanov, V., & Steinhardt, P.J. 2000, Phys. Rev. Lett., 85, 4438
- Armitage, P.J., & Natarajan, P. 2002, ApJ, 567, L9
- Arun, K. G., Blanchet, L., Iyer, B. R., & Qusailah, M. S. S. 2004, Class. Quan. Grav. 21, 3771
- Barack, L., & Cutler, C. 2004, Phys. Rev. D, 69, 082005
- Begelman, M.C., Blandford, R.D., & Rees, M.J. 1980, Nature, 287, 307
- Blanchet, L. 2002, Living Rev. Relativity, 5, 3
- Blanchet, L., Damour, T., Esposito-Farese, G., & Iyer, B. R. 2004 Phys. Rev. Lett., 93, 091101
- Caldwell, R., Dave, R., & Steinhardt, P.J. 1998, Phys. Rev. Lett., 80, 1582
- Chernoff, D.F., & Finn, L.S. 1993, ApJ, 411, L5
- Cutler, C. 1998, Phys. Rev. D, 57, 7089
- Cutler, C. & Flanagan, E.F. 1993, Phys. Rev. D, 49, 2658
- Dalal, N., Holz, D.E., Chen, X., & Frieman, J.A. 2003, ApJ, 585, L11
- Danzmann, K., et al. 1998, *LISA—Laser Interferometer Space Antenna, Pre-Phase A Report*, Max-Planck-Institut für Quantenoptik, Report MPQ 233
- Drell, P., Loredo, T.J., & Wasserman, I. 2000, ApJ, 530, 593
- Finn, L.S. 1992, Phys. Rev. D, 46, 5236
- Finn, L.S. 1996, Phys. Rev. D, 53, 2878
- Finn, L.S. & Chernoff, D.F. 1993, Phys. Rev. D, 47, 2198
- Haehnelt, M.G. 1998, in *Laser Interferometer Space Antenna—2nd International LISA Symposium on the Detection and Observation of Gravitational Waves in Space*, AIP Conf. Proc. Vol. 456, edited by W. M. Folker (AIP, New York, 1998)
- Holz, D.E. & Linder, E.V. 2005, astro-ph/0412173
- Holz, D.E. & Wald, R.M. 1998, Phys. Rev. D, 58, 063501
- Hu, W. 1999, ApJ, 522, L21
- Hughes, S.A. 2002, MNRAS, 331, 805
- Hughes, S.A. 2003, Annals Phys., 303, 142
- Kaiser, N. 1992, ApJ, 388, 272
- Knop, R.A. et al. 2003, ApJ, 598, 102
- Kocsis, B., Frei, Z., Haiman, Z., & Menou, K. 2005, in preparation
- Lehto, H.J., & Valtonen, M.J. 1996, ApJ, 460, 207
- Marković, D. 1993, Phys. Rev. D, 48, 4738
- Metcalf, R.B., & Silk, J. 1999, ApJ, 519, L1
- Milosavljević, M. & Phinney, E.S. 2004, ApJ, submitted.
- Moore, T.A., & Hellings, R.W. 2002, Phys. Rev. D, 65, 062001
- Perlmutter, S., et al. 1999, ApJ, 517, 565
- Phillips, M.M. 1993, ApJ, 413, L105
- Poisson, E., & Will, C.M. 1995, Phys. Rev. D, 52, 848
- Richstone, D. 1998, in *Laser Interferometer Space Antenna—2nd International LISA Symposium on the Detection and Observation of Gravitational Waves in Space*, AIP Conf. Proc. 456, edited by W. M. Folkner (AIP, New York, 1998).
- Riess, A.G., Press, W.H., & Kirshner, R.P. 1995, ApJ, 438, L17
- Riess, A., et al. 1998, AJ, 116, 1009
- Schutz, B.F. 1986, Nature, 323, 310
- Schutz, B.F., in *Lighthouses of the Universe—Proceedings of the MPA/ESO*, p. 207; gr-qc/0111095
- Seljak, U., & Holz, D.E. 1999, A&A, 351, L10
- Seto, N 2002, Phys. Rev. D, 66, 122001
- Sillanpää, A., Haarala, S., Valtonen, M.J., Sundelius, B., & Byrd, G.G. 1988, ApJ, 325, 628
- Spiegel, D.N., et al. 2003, ApJS, 148, 175
- Takahashi, R., & Nakamura, T. 2003; astro-ph/0305055
- Tonry, J.L. et al. 2003, ApJ, 594, 1
- Vecchio, A. 2004, Phys. Rev. D, 70, 042001
- Volonteri, M., Haardt, F., & Madau, P. 2003, ApJ, 582, 559
- Wang, L., Goldhaber, G., Aldering, G., & Perlmutter, S. 2003, ApJ, 590, 944
- Wang, Y., Holz, D.E., & Munshi, D. 2002, ApJ, 572, L15
- Wang, Y., Stebbins, A., & Turner, E.L. 1996, Phys. Rev. Lett., 77, 2875
- Wang, Y., & Turner, E.L. 1997, Phys. Rev. D, 56, 724
- Williams, R.E., et al. 1996, ApJ, 112, 4



TABLE 1  
MEASUREMENT PRECISION AT  $z = 1$  WITH  $f_{\text{low}} = 10^{-4}$  Hz

$m_1 (M_\odot)$	$m_2 (M_\odot)$	$\delta D_L/D_L$ (5%, 25%, 50%, 90%)	$\delta\theta$ (5%, 25%, 50%, 90%)
$10^4$	$10^4$	(0.005, 0.010, 0.014, 0.042)	(14.3, 28.3, 48.5, 117) arcmin
$10^4$	$3 \times 10^4$	(0.003, 0.008, 0.013, 0.037)	(11.0, 22.1, 41.6, 111) arcmin
$10^4$	$6 \times 10^4$	(0.003, 0.007, 0.013, 0.036)	(9.05, 19.1, 40.4, 109) arcmin
$10^4$	$10^5$	(0.005, 0.007, 0.013, 0.035)	(7.85, 18.3, 39.5, 110) arcmin
$3 \times 10^4$	$10^5$	(0.002, 0.006, 0.013, 0.029)	(5.26, 14.6, 37.4, 120) arcmin
$6 \times 10^4$	$10^5$	(0.002, 0.006, 0.012, 0.037)	(4.07, 12.9, 35.0, 120) arcmin
$10^5$	$10^5$	(0.002, 0.005, 0.012, 0.034)	(3.36, 11.7, 33.4, 117) arcmin
$10^5$	$3 \times 10^5$	(0.001, 0.005, 0.012, 0.035)	(2.71, 10.6, 33.1, 116) arcmin
$10^5$	$6 \times 10^5$	(0.001, 0.006, 0.014, 0.044)	(2.82, 12.0, 38.8, 120) arcmin
$10^5$	$10^6$	(0.002, 0.009, 0.017, 0.053)	(3.89, 18.5, 50.9, 126) arcmin
$3 \times 10^5$	$10^6$	(0.002, 0.013, 0.026, 0.087)	(4.65, 29.7, 71.0, 172) arcmin
$6 \times 10^5$	$10^6$	(0.003, 0.019, 0.035, 0.122)	(5.60, 39.2, 93.6, 220) arcmin
$10^6$	$10^6$	(0.004, 0.024, 0.043, 0.149)	(6.36, 52.2, 118, 271) arcmin

TABLE 2  
MEASUREMENT PRECISION AT  $z = 1$  WITH  $f_{\text{low}} = 3 \times 10^{-5}$  Hz

$m_1 (M_\odot)$	$m_2 (M_\odot)$	$\delta D_L/D_L$ (5%, 25%, 50%, 90%)	$\delta\theta$ (5%, 25%, 50%, 90%)
$10^5$	$10^5$	(0.002, 0.005, 0.012, 0.036)	(3.35, 11.4, 33.2, 117) arcmin
$10^5$	$3 \times 10^5$	(0.001, 0.005, 0.011, 0.034)	(2.68, 10.4, 31.0, 107) arcmin
$10^5$	$6 \times 10^5$	(0.001, 0.005, 0.010, 0.032)	(2.71, 9.85, 29.7, 103) arcmin
$10^5$	$10^6$	(0.001, 0.005, 0.010, 0.031)	(3.27, 10.5, 29.1, 101) arcmin
$3 \times 10^5$	$10^6$	(0.001, 0.004, 0.009, 0.028)	(2.45, 8.77, 25.8, 89.9) arcmin
$6 \times 10^5$	$10^6$	(0.001, 0.004, 0.009, 0.026)	(2.25, 8.5, 24.8, 84.3) arcmin
$10^6$	$10^6$	(0.001, 0.004, 0.009, 0.026)	(2.39, 9.05, 25.3, 83.5) arcmin
$10^6$	$3 \times 10^6$	(0.002, 0.006, 0.011, 0.034)	(4.56, 12.6, 34.6, 93.8) arcmin
$10^6$	$6 \times 10^6$	(0.003, 0.008, 0.016, 0.051)	(7.16, 20.6, 45.9, 110) arcmin
$10^6$	$10^7$	(0.003, 0.011, 0.021, 0.071)	(9.20, 27.0, 57.1, 136) arcmin

TABLE 3  
MEASUREMENT PRECISION AT  $z = 3$  WITH  $f_{\text{low}} = 10^{-4}$  Hz

$m_1 (M_\odot)$	$m_2 (M_\odot)$	$\delta D_L/D_L$ (5%, 25%, 50%, 90%)	$\delta\theta$ (5%, 25%, 50%, 90%)
$10^4$	$10^4$	(0.013, 0.029, 0.051, 0.143)	(37.7, 78.2, 158, 422) arcmin
$10^4$	$3 \times 10^4$	(0.010, 0.026, 0.050, 0.135)	(27.2, 66.8, 150, 428) arcmin
$10^4$	$6 \times 10^4$	(0.008, 0.024, 0.050, 0.145)	(22.0, 57.7, 140, 442) arcmin
$10^4$	$10^5$	(0.008, 0.024, 0.050, 0.142)	(19.3, 55.4, 143, 465) arcmin
$3 \times 10^4$	$10^5$	(0.006, 0.019, 0.044, 0.131)	(12.6, 44.5, 125, 444) arcmin
$6 \times 10^4$	$10^5$	(0.006, 0.021, 0.044, 0.128)	(10.1, 42.6, 132, 429) arcmin
$10^5$	$10^5$	(0.005, 0.024, 0.049, 0.141)	(9.55, 44.8, 144, 430) arcmin
$10^5$	$3 \times 10^5$	(0.007, 0.034, 0.069, 0.213)	(11.3, 69.9, 193, 485) arcmin
$10^5$	$6 \times 10^5$	(0.008, 0.044, 0.087, 0.287)	(17.5, 96.1, 240, 593) arcmin
$10^5$	$10^6$	(0.009, 0.058, 0.111, 0.378)	(23.4, 127, 304, 734) arcmin

TABLE 4  
 MEASUREMENT PRECISION AT  $z = 3$  WITH  $f_{\text{low}} = 3 \times 10^{-5}$  Hz

$m_1 (M_\odot)$	$m_2 (M_\odot)$	$\delta D_L / D_L$ (5%, 25%, 50%, 90%)	$\delta\theta$ (5%, 25%, 50%, 90%)
$10^4$	$10^4$	(0.013, 0.029, 0.050, 0.136)	(37.4, 76.0, 156, 423) arcmin
$10^4$	$3 \times 10^4$	(0.010, 0.026, 0.050, 0.137)	(26.5, 62.7, 149, 437) arcmin
$10^4$	$6 \times 10^4$	(0.009, 0.024, 0.049, 0.140)	(21.9, 57.8, 141, 441) arcmin
$10^4$	$10^5$	(0.007, 0.023, 0.049, 0.139)	(19.0, 55.3, 143, 465) arcmin
$3 \times 10^4$	$10^5$	(0.006, 0.019, 0.043, 0.135)	(12.4, 43.6, 124, 429) arcmin
$6 \times 10^4$	$10^5$	(0.005, 0.018, 0.040, 0.126)	(10.4, 38.8, 114, 404) arcmin
$10^5$	$10^5$	(0.004, 0.016, 0.038, 0.120)	(8.85, 34.7, 106, 384) arcmin
$10^5$	$3 \times 10^5$	(0.004, 0.016, 0.035, 0.108)	(8.26, 32.4, 98.7, 360) arcmin
$10^5$	$6 \times 10^5$	(0.005, 0.016, 0.035, 0.105)	(10.9, 36.0, 100, 346) arcmin
$10^5$	$10^6$	(0.006, 0.017, 0.035, 0.106)	(15.2, 41.6, 105, 349) arcmin
$3 \times 10^5$	$10^6$	(0.005, 0.017, 0.034, 0.100)	(12.2, 37.3, 101, 327) arcmin
$6 \times 10^5$	$10^6$	(0.006, 0.019, 0.039, 0.115)	(13.1, 42.1, 120, 336) arcmin
$10^6$	$10^6$	(0.007, 0.025, 0.049, 0.146)	(16.9, 55.5, 145, 359) arcmin
$10^6$	$3 \times 10^6$	(0.009, 0.040, 0.077, 0.240)	(24.8, 89.1, 208, 507) arcmin
$10^6$	$6 \times 10^6$	(0.014, 0.063, 0.116, 0.392)	(35.4, 142, 322, 757) arcmin